First-principles study of transparent *p*-type conductive $SrCu_2O_2$ and related compounds

Xiliang Nie, Su-Huai Wei, and S. B. Zhang
National Renewable Energy Laboratory, Golden, Colorado 80401
(Received 5 October 2001; published 31 January 2002)

Using first-principles band structure methods we have systematically studied the electronic and optical properties of *p*-type transparent conductive oxides $SrCu_2O_2$ and related compounds $A^{II}Cu_2O_2$, where A = Mg, Ca, and Ba, as well as their host material Cu_2O. We show that all these compounds have direct band gap at the zone center (Γ) with $SrCu_2O_2$ having the largest band gap. The trend of band gap variation of $A^{II}Cu_2O_2$ as a function of A^{II} is explained in terms of atomic energy levels and atomic sizes of the A^{II} elements. Transparency of $SrCu_2O_2$ is explained by the calculated dipole transition matrix elements. The calculated effective masses for the conduction band states are found to be larger than those for the valence states for $SrCu_2O_2$, opposite to the trend in conventional semiconductors and *n*-type transparent conductive oxides. We predict that adding a small amount of Ca (~16%) into $SrCu_2O_2$ can increase the band gap and reduce the hole effective mass of $SrCu_2O_2$, therefore, increase the transparency and conductivity.

DOI: 10.1103/PhysRevB.65.075111 PACS number(s): 71.20.−b, 78.20.−e

I. INTRODUCTION

Transparent conductive oxides (TCO's) is a group of materials with unique physical properties.[1] Despite their large band gaps (>3 eV), thus transparent under normal conditions, the TCO's can sustain a high concentration of charged carriers and also maintain a high mobility. They are widely used as transparent electrodes in flat panel displays, solar cells, and touch panels. Almost all of the well known TCO's such as ZnO, In_2O_3, SnO_2, and their alloys have *n*-type conductivity. This can be attributed to the fact that the valence band maximum (VBM) states of these TCO's are mainly O *p* states with very high ionization energies. Consequently, according to the recently developed doping limit rule,[2] it will be very difficult to dope them *p* type. The lack of *p*-type TCO's severely limits the potential applications of these materials, for instance, as transparent diodes. Currently there are considerable interests in finding *p*-type TCO's and understanding the *p*-type doping mechanism.

Recently, several Cu containing oxides such as $CuAlO_2$ and $SrCu_2O_2$ have been proposed[3] to be good candidates for *p*-type TCO's. It is based on the observations that the prototype Cu containing oxide, Cu_2O is a well-known *p*-type semiconductor with, however, somewhat small band gap of 2.1 eV. Cu has shallow, occupied $3d$ orbitals close to the O $2p$ orbitals. Thus, the VBM states will be mostly Cu *d* like. The coupling between the Cu *d* states and the O *p* states leads to smaller ionization energies (which is equivalent to higher VBM) for these Cu compounds than conventional oxides, thus, making it easier to dope them *p* type. By modifying the crystal structure of Cu_2O, e.g., reducing the oxygen mediated *d*-*d* coupling between the Cu atoms, it is possible to enlarge the band gap,[4,5] thus enhance the transparency of Cu containing oxides.

In this work, using first-principles band structure methods, we have calculated the electronic and optical properties of $SrCu_2O_2$. We investigate the origin of the transparency and *p*-type conductivity in $SrCu_2O_2$ and related compounds such as Cu_2O and $A^{II}Cu_2O_2$, where A^{II} = Mg, Ca, and Ba. Among these compounds, $BaCu_2O_2$ is known[6] to exist in the same crystal structure as $SrCu_2O_2$.[7] However $MgCu_2O_2$ and $CaCu_2O_2$ have yet to be synthesized. We find that both $SrCu_2O_2$ and Cu_2O are direct band gap materials with their band edges at the zone center (Γ). Adding SrO into Cu_2O reduces the *d*-*d* coupling between the Cu atoms and raises the band gap by 1.31 eV, in good agreement with the experimental value of 1.22 eV. The top of the valence band in $SrCu_2O_2$ is found to be mostly Cu *d* and O *p*. The calculated dipole transition matrix elements show that transition between the VBM and other valence states is negligible within 4 eV below the VBM. This is crucial for *p*-type TCO's as large fundamental gap is not enough to guarantee transparency. The bottom of the conduction band minimum (CBM) is mostly Cu *d* and O *p* with some Sr *s*. The calculated effective masses for the conduction band states are found to be larger than those for the valence states, opposite to the trend in conventional semiconductors and *n*-type TCO's. These results are explained in terms of the coupling between Cu *d* states and O *p* states. For $A^{II}Cu_2O_2$ we found that they all have direct band gaps at Γ. The predicted band gaps are 2.45, 3.01, 3.33, and 3.01 eV, for $MgCu_2O_2$, $CaCu_2O_2$, $SrCu_2O_2$, and $BaCu_2O_2$, respectively. In the following, we discuss briefly our calculation methods and the sailient features of our calculated results.

II. CRYSTAL STRUCTURE

The crystal structure of Cu_2O is shown in Fig. 1(a). It is cubic with a space group O_h^4. The O atoms occupy the positions in a body-centered cube and Cu atoms stay in the positions in a face-centered cube. The measured[8] lattice constant is a = 4.2696 Å, so the Cu-O bond length is 1.85 Å. Instead, $SrCu_2O_2$ has a tetragonal structure with space group of $I4_1/amd$ [Fig. 1(b)]. The measured lattice constants are a = 5.48 Å and c = 9.82 Å, respectively.[7] In this crystal structure, Sr atoms are at the center of a distorted octahedron formed by O atoms. The nearest-neighbor (NN) Sr-O bond length along the c direction is $R_{NN}(\text{Sr-O}) = uc$, where u is the internal structural parameter, and the next-nearest-neighbor (*NNN*) Sr-O distance is slightly larger, given by

$$R_{NNN}(\text{Sr-O}) = \sqrt{(0.25-u)^2c^2 + 0.25a^2}. \quad (1)$$

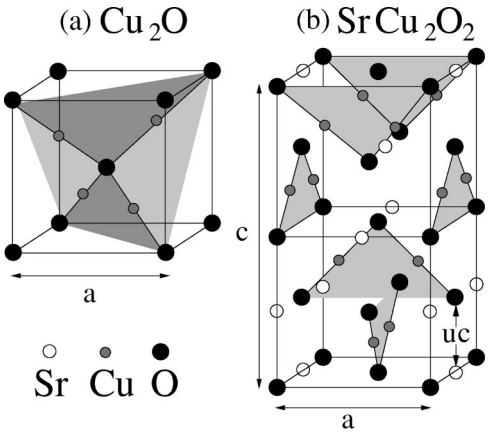

FIG. 1. Crystal structure of (a) Cu_2O and (b) $SrCu_2O_2$.

In the ideal structure with $c=2a$ and $u=0.25$, the two bond lengths R_{NN} and R_{NNN} are equal. The Cu atoms form the well-known O-Cu-O dumbbell configuration. The nearest-neighbor Cu-O bond length is given by

$$R_{NN}(\text{Cu-O})=\sqrt{(0.0375-u)^2c^2+0.0625a^2}. \tag{2}$$

This dumbbell O-Cu-O unit is similar to that of Cu_2O. In fact, $SrCu_2O_2$ can be considered as being derived from Cu_2O_2, where one Cu atom is removed for each unit of distorted Cu_2O, plus an inter-penetrating body centered tetragonal Sr sublattice.

However, unlike the three-dimensional dumbbell structure in Cu_2O, the O-Cu-O dumbbells in $SrCu_2O_2$ are connected to form one-dimensional zigzag chains along the [100] and [010] directions, respectively. The angle between them is given by

$$\tan(\theta/2)=\frac{a}{(1.5-4u)c}. \tag{3}$$

For $SrCu_2O_2$, the measured internal structural parameter is close to the ideal value of $u=0.25$, so the angle $\theta=96.3°$. This value is smaller than the tetrahedral angle of $\theta=109.5°$ in Cu_2O. However, the Cu-O bond length of 1.84 Å in $SrCu_2O_2$ remains nearly the same as in Cu_2O. We will show later that this change from three-dimensional O-Cu-O chain in Cu_2O to one-dimensional chain in $SrCu_2O_2$ reduces the O mediated Cu-Cu interactions, thus narrowing the *d* band width and increasing the band gap for $SrCu_2O_2$.

III. METHOD OF CALCULATION

The total energy calculation is performed using the local density approximation (LDA) (Ref. 9) as implemented by the general potential linearized augmented plane wave method.[10] No shape approximation was used for either the potential or the charge density. We used muffin-tin radii of 2.5, 2.0, and 1.4 Bohr for A^{II}, Cu, and O atoms respectively. The basis set cutoff energy is 23 Ry. The Ca $3p$, Sr $4p$, and Ba $5p$ states are treated as valence states. Spin-orbit coupling which is implemented by using the second-variation method[11] is included when calculating the effective mass. To determine the structure parameters, we first search for the minimum total energy with respect to *a*, *c*, and *u* at fixed volume. The ground state properties were then extracted from these calculated minimum total energies at each volume, fitting to the Murnaghan equation of state.[12] The Brillouin-zone integrations were performed using 20 special **k** points[13] for the cubic Cu_2O structure and 15 special **k** points for the tetragonal $A^{II}Cu_2O_2$ structure in the irreducible Brillouin zone. To calculate the density of states, larger numbers of **k** points are used. We used the Ceperley-Alder exchange correlation potentials[14] as parametrized by Perdew and Zunger.[15] The optical properties of these materials are studied by calculating the dipole matrix element

$$M_{\text{VBM},j}(\mathbf{k})=|\langle\psi_{\text{VBM},\mathbf{k}}|\mathbf{P}|\psi_{j,\mathbf{k}}\rangle|^2 \tag{4}$$

at $\mathbf{k}=0$ using the optic package[16] in the WIEN97 code.[17]

IV. RESULTS AND DISCUSSIONS

A. Structural parameters

Table I presents the calculated structural parameters for Cu_2O and $A^{II}Cu_2O_2$ (A^{II}=Mg, Ca, Sr, and Ba). The calculated results are compared with available experimental data.[6,7] The agreements are very good. The slight underestimate of the calculated lattice constant *a* by less than 2% is

TABLE I. Calculated structural parameters and semirelativistic band gaps for cubic Cu_2O and tetragonal $A^{II}Cu_2O_2$ (A^{II}=Mg, Ca, Sr, and Ba). The calculated spin-orbit splitting Δ_0 for Cu_2O is -0.127 eV. To correct the LDA band gap errors we added a constant of 1.5 eV to the LDA calculated band gaps. The predicted band gaps are given as $E_g^{\text{LDA}+C}$. The calculated results are compared with available experimental (exp.) data.

	a(Å)	c(Å)	θ	u	$l_{\text{Cu-O}}$(Å)	E_g^{LDA} (eV)	$E_g^{\text{LDA}+C}$ (eV)
Cu_2O	4.216	4.216	109.5		1.826	0.52	2.02
exp.	4.270	4.270	109.5		1.849		2.10
$MgCu_2O_2$	5.078	8.951	87.2	0.226	1.841	0.95	2.45
$CaCu_2O_2$	5.290	9.336	93.2	0.241	1.821	1.51	3.01
$SrCu_2O_2$	5.406	9.729	95.6	0.249	1.825	1.83	3.33
exp.	5.480	9.820	96.3	0.250	1.840		3.30
$BaCu_2O_2$	5.650	9.935	102.1	0.260	1.817	1.51	3.01
exp.	5.722	10.064					

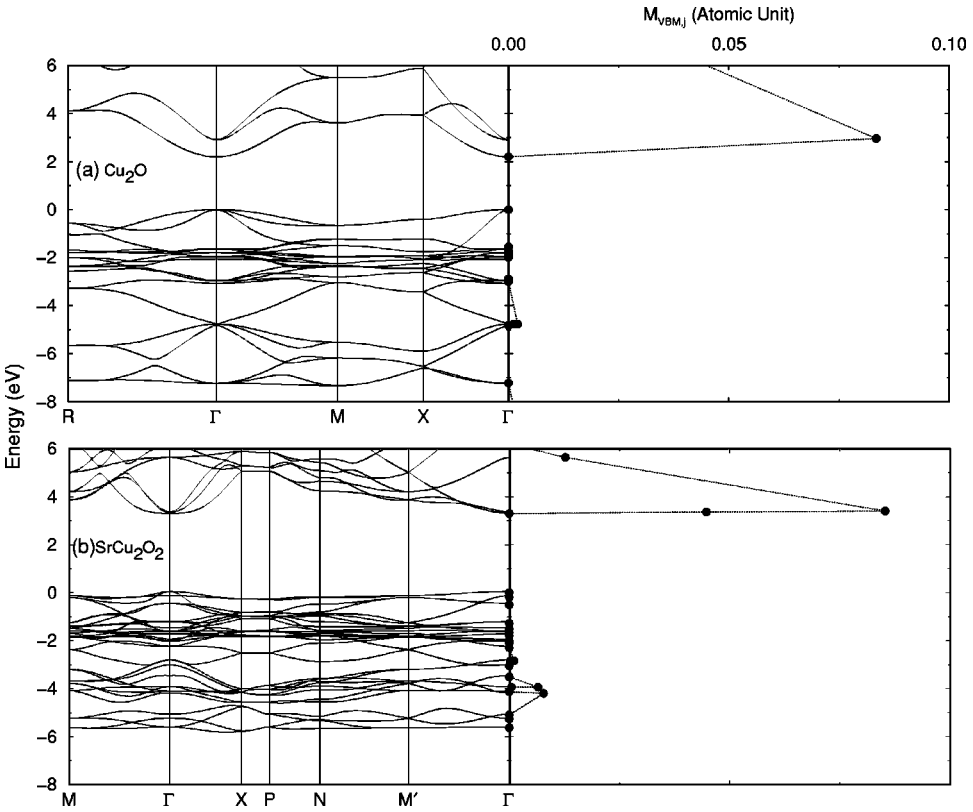

FIG. 2. Calculated semirelativistic electronic band structure for (a) Cu_2O and (b) $SrCu_2O_2$ and the dipole transition matrix elements between the VBM and other states at Γ. Energy zero is at VBM. The energy of the conduction bands are shifted upwards by 1.5 eV to correct the LDA band gap error.

typical for the LDA calculations. As expected, the lattice constants increase as the size of the A^{II} atoms increase from Mg, Ca, Sr, to Ba. It is important to see that in $A^{II}Cu_2O_2$ the nearest neighbor Cu-O bond lengths are nearly independent of A^{II} and are very close to that in Cu_2O. It suggests that the bonding characters between Cu and O are very similar in this group of compounds. The conservation of the Cu-O bond length in $A^{II}Cu_2O_2$ is made possible by the displacement of the O atoms away from their ideal position at $u=0.25$. Only $SrCu_2O_2$ has a $u=0.249$ close to the ideal value. The displacement of the O atoms also leads to a change in the O-Cu-O dumbbell bond angle θ. This leads to an increase of θ when the atomic numbers of A^{II} increases. However, the bond angle θ in $A^{II}Cu_2O_2$ remains to be significantly smaller than the tetrahedral bond angle $\theta=109.5°$ in Cu_2O. This is because to accommodate the A^{II}-O bond length which is absent in Cu_2O, the system would like to have c/a ratio close to two, so the angle θ close to 90°.

B. Band structures and DOS of $SrCu_2O_2$ and Cu_2O

The calculated band structure of $SrCu_2O_2$ at the experimental lattice constants along some high symmetry directions is shown in Fig. 2(b). For comparison, we also show in Fig. 2(a) the calculated band structure of Cu_2O. It shows that $SrCu_2O_2$ has a direct band gap at Γ. The LDA calculated band gap of 1.83 eV is about 1.47 eV smaller than experimental value of 3.3 eV. Cu_2O also has a direct band gap at Γ. The LDA calculated band gap of 0.52 eV is about 1.58 eV smaller than the experimental value of 2.1 eV. However, the calculated band gap difference of 1.31 eV between $SrCu_2O_2$ and Cu_2O is in very good agreement with experimental value. Based on this observation, we assume that the LDA band gap errors of $\sim$1.5 eV is independent of the A^{II} atoms due to the similarity of the characters of the band edge states. A uniform upward shift of the conduction band by 1.5 eV is included in Fig. 2.

Figure 3 plots the total electron density of states (DOS) and the site- and angular-momentum projected local (within the muffin-tin spheres) DOS for $SrCu_2O_2$. We see that the valence states consist of two major parts: The upper part from the VBM to $E_{\rm VBM}-3$ eV consists predominantly the Cu $3d$ states. The lower part from $E_{\rm VBM}-3$ eV to $E_{\rm VBM}-6$ eV consists predominantly the O $2p$ states. This is due to the fact that Cu $3d$ level is shallower than O $2p$. Thus, the Cu containing oxides such as Cu_2O have much higher VBM than other conventional oxides such as ZnO, where the Zn $3d$ state is deeper than the O $2p$ state. Higher VBM also leads to higher *p*-type dopability as suggested by the doping limit rule. Figure 3 also shows that there are significant hybridization between the Cu $3d$ and O $2p$ states in the valence bands. The contribution of Sr orbitals to the valence band is, however, much weaker.

To understand the large band gap of $SrCu_2O_2$ relative to Cu_2O, we plot in Fig. 4 the DOS and local DOS for Cu_2O. We see that the DOS of Cu_2O is similar to that of $SrCu_2O_2$. However, in $SrCu_2O_2$ the O mediated Cu-Cu interaction is one dimensional, while in Cu_2O the interaction is three dimensional. Therefore, the upper valence band width in $SrCu_2O_2$ is much narrower than that in Cu_2O. This lowers the VBM, thus leads to the opening up of the band gap in $SrCu_2O_2$. To test this theory further, we have calculated the band gap of $(Cu_2O_2)^{-2}$ which has the same crystal structure

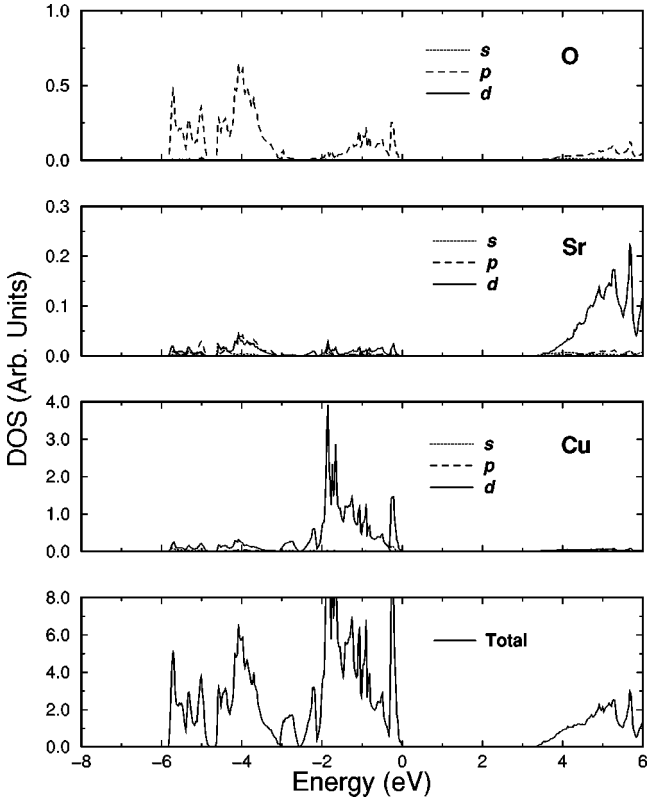

FIG. 3. Calculated total and local density of states (DOS) for $SrCu_2O_2$.

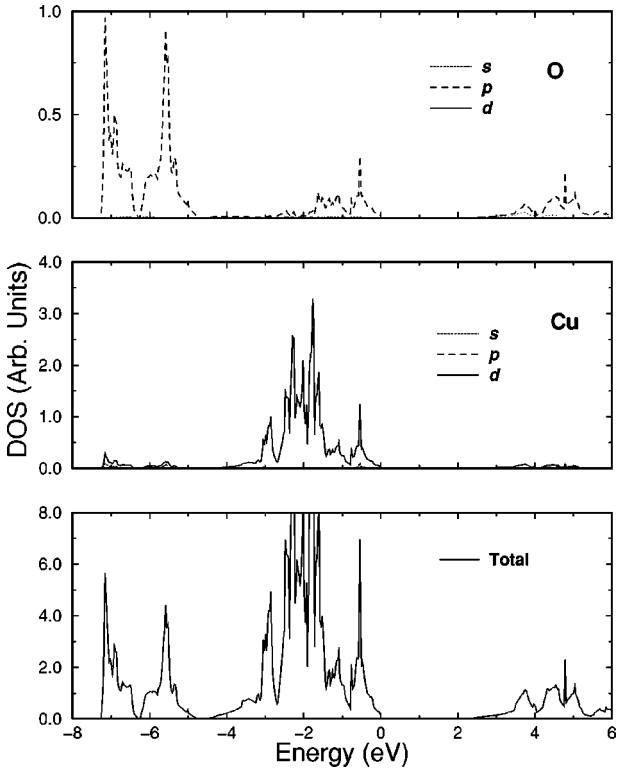

FIG. 4. Calculated total and local density of states (DOS) for Cu_2O.

and structural parameters as for $SrCu_2O_2$, except that one Sr atom is replaced by a vacancy with two valence electrons ($q=-2$). To keep the charge neutrality of the cell, positively charged, uniform jellium background is included. Indeed, we find that the LDA band gap of $(Cu_2O_2)^{-2}$ is 1.79 eV that is close to the 1.83 eV for $SrCu_2O_2$. Its upper valence band width is also very close to that for $SrCu_2O_2$. These results show clearly that the band gap opening is due to the narrowing of the Cu *d* band by the one-dimensional O-Cu-O dumbbell structure. This finding is consistent with the early assumption of Kudo and co-workers.[3,18]

C. Optical properties of $SrCu_2O_2$ and Cu_2O

In order to be transparent, a *p*-type TCO not only should have a large fundamental band gap, so no visible light absorption between the valence bands and the conduction bands can take place, but also it should have no visible light absorption between the VBM and the bands below. A look of the band structure of $SrCu_2O_2$ in Fig. 2(b) shows, however, that there are many bands within 3 eV below the VBM. It is, therefore, surprising to have *p*-type $SrCu_2O_2$ transparent. To understand this paradox, we have calculated the dipole transition matrix elements between the VBM state and other states at Γ. The results are shown in the right panel of Fig. 2. We find that indeed, the dipole transition probabilities between the VBM and the other states within 4 eV below the VBM are negligible. This is because the on-site transition from same angular momentum (such as O *p* to O *p* and Cu *d* to Cu *d*) is forbidden according to the classical selection rule. This explains the transparency for this *p*-type material. It is interesting to see that the direct dipole transition from the VBM state to the CBM state is also forbidden, similar to that found in Cu_2O [Fig. 2(a)]. This has been explained by Elliott[19] and Ching *et al.*[20] due to a phase cancellation for compounds with nonsymmophic space group.

D. Effective mass of $SrCu_2O_2$ and Cu_2O

A *p*-type TCO with good conductivity should have high mobility, thus, small hole effective mass. To test this, the electron and hole effective masses for Cu_2O and $SrCu_2O_2$ are calculated along high symmetry directions.

For the cubic Cu_2O the effective masses at Γ are calculated along the $\Gamma-X$ $(2\pi/a)(\frac{1}{2}00)$, $\Gamma-M$ $(2\pi/a)(\frac{1}{2}\frac{1}{2}0)$, and $\Gamma-R$ $(2\pi/a)(\frac{1}{2}\frac{1}{2}\frac{1}{2})$ directions. The results are show in Table II and are compared with available experimental data.[21–23] We find that the electron effective masses are essentially isotropic, while the hole effective masses are anisotropic, especially for the heavy hole state. Because Cu_2O has a negative spin-orbit splitting ($\Delta_0=-0.127$ eV) at Γ, the top of the valence band is a light hole state with its effective mass even smaller than the CBM state. This is in contrast to most conventional semiconductors and *n*-type TCO's where the electron effective mass is much smaller than the hole effective mass. Our calculated effective masses are slightly smaller than the available experimental values. This is typical for LDA calculations and is related to the underestimation of the band gap. Our calculated results, however, are

TABLE II. Calculated electron and valence bands effective masses (in unit of free electron mass m_0) at Γ along Γ-X, Γ-M, and Γ-R directions and energy levels ε_{SO} (in eV) with spin-orbital coupling for Cu_2O. For the valence states the order (in decreasing energy) is light hole (LH), heavy hole (HH), and spin-orbit split-off hole (SPH). Results are calculated at experimental lattice constant and is compared with available experimental data.

		ε_{SO}	ΓX	ΓM	ΓR	Average	Expt.
CBM		0.44	0.92	0.92	0.92	0.92	0.99 [a], 0.98 [b]
VBM	(LH)	0.00	0.36	0.36	0.36	0.36	0.58 [a], 0.69 [b]
	(HH)	−0.13	2.83	0.91	0.72	1.49	
	(SPH)	−0.13	0.21	0.25	0.27	0.24	

[a]Reference 23.

[b]Reference 21.

significantly different from the theoretical prediction of Ching *et al.*[20] and Ruiz *et al.*[24] For example, Ruiz *et al.*[24] found the heavy hole effective mass to be $28.7m_0$, whereas Ching *et al.*[20] found it to be 3.02, both are much larger than our calculated value of $1.49m_0$. Part of the reason for the discrepancy is due to the negalect of the spin-orbit interation in their calculations. Spin-orbital coupling mixes wave functions at the top of valence band, thus, has very large effects on the calculated effective masses.

For the tetragonal $SrCu_2O_2$ the effective masses at Γ are calculated along the Γ-M $(2\pi/a)(100)$, $\Gamma - M'$ $(2\pi/c)\times(002)$ directions. The results are show in Table III. Again, we see that for this *p*-type material, the effective mass of the CBM is much larger than that of the VBM. Both the electron effective masses and the hole effective masses are anisotropic. The hole effective masses along the *c* axis ($\Gamma M'$) are much larger than the one perpendicular to the *c* axis (ΓM). These results indicate that for single crystal, which could be obtained by epitaxial growth, electrical conductivity perpendicular to the *c*-axis will be much larger than that parallel to the *c* axis.

E. Chemical trend of the band gap of $A^{II}Cu_2O_2$ compounds

To search for a better *p*-type TCO's and to understand the effects of the Sr atom in $SrCu_2O_2$, we have calculated the band structures of $A^{II}Cu_2O_2$ where A=Mg, Ca, Sr, and Ba. The calculated band structures are plotted in Fig. 5, where the conduction bands are shifted upwards by 1.5 eV to correct the LDA errors. All the four compounds show direct band gaps at Γ. The calculated minimum band gaps for these four compounds are given in Table I. We see that the variation of the band gaps of $A^{II}Cu_2O_2$ is nonmonotonic. The band gaps increase from $MgCu_2O_2$ to $CaCu_2O_2$ to $SrCu_2O_2$, but it becomes smaller when Sr is replaced by Ba.

To analyze the variation of the band gaps in these systems, we have decomposed the change of the band gap into two parts: chemical and size contributions when moving away from $SrCu_2O_2$. The chemical contribution is due to the replacement of Sr atom by A^{II} atoms with different atomic chemical potentials. This effect is studied by calculating the band structure of the four $A^{II}Cu_2O_2$ compounds at fixed $SrCu_2O_2$ lattice constant. The calculated eigenvalues of the band edge states at Γ and their angular momentum and size decomposed charge distributions are listed in Table IV. We find that the VBM of these compounds all have the Γ_5 symmetry (doubly degenerate without spin), except for $BaCu_2O_2$ that has a symmetry of Γ_2 (singly degenerate). The CBM states all have the Γ_1 symmetry, except for $BaCu_2O_2$ that has a Γ_1' symmetry. For the valence bands, the Γ_5 state is predominately the Cu $3d$ and O $2p$ state with negligible A^{II} contribution, thus, the energy level of the Γ_5 state is not sensitive to the substitution of different A^{II} atoms. The Γ_2 state, however, contains significant contributions from the A^{II} p levels. Thus, when the p orbital energies of the A^{II} atom increases monotonically from Mg, Ca, Sr, to Ba (Fig. 6), the Γ_2 energy level also increases. For $BaCu_2O_2$, the Γ_2 level moves above the Γ_5 level, thus, become the VBM. For the conduction bands, the Γ_1 state contains significant contribution from the A^{II} atomic s orbitals, while the Γ_1' state has significant contribution from the A^{II} atomic d orbitals, therefore, it is not surprising to see that the energy levels of the Γ_1 and Γ_1' states follow the same trends as the respective atomic orbital energies of the A^{II} atoms. The Γ_1 energy level increases from Mg to Ba, while the Γ_1' level, in general, decreases from Mg to Ba. For $BaCu_2O_2$, the Γ_1' energy level is below the Γ_1 energy level. Therefore the reduction

TABLE III. Calculated effective masses (in m_0) at Γ along high symmetry directions and energy levels ε_{SO} and ε_{NSO} (all energy level is relative to their semirelativisitic Γ_5 states in eV) with or without spin-orbital coupling for $A^{II}Cu_2O_2$ (A^{II}=Mg, Ca, Sr, Ba). For $SrCu_2O_2$ and $BaCu_2O_2$ the results are calculated at experimental lattice constants. For $CaCu_2O_2$ and $MgCu_2O_2$ where experimental data are not available, we used our calculated equilibrium lattice parameters.

	$MgCu_2O_2$				$CaCu_2O_2$				$SrCu_2O_2$				$BaCu_2O_2$			
	ε_{NSO}	ε_{SO}	ΓM	$\Gamma M'$	ε_{NSO}	ε_{SO}	ΓM	$\Gamma M'$	ε_{NSO}	ε_{SO}	ΓM	$\Gamma M'$	ε_{NSO}	ε_{SO}	ΓM	$\Gamma M'$
Γ_2	−0.52	−0.54	19.68	0.25	−0.26	−0.28	3.30	0.32	−0.17	−0.20	2.40	0.44	0.09	0.15	1.78	0.39
Γ_5	0.00	0.00	0.28	1.81	0.00	0.02	0.44	1.46	0.00	−0.02	0.48	2.12	0.00	−0.15	0.83	1.10
	0.00	0.02	0.27	3.17	0.00	0.03	0.39	2.91	0.00	0.03	0.57	1.27	0.00	0.08	0.66	3.34
Γ_1	1.05	1.05	1.79	0.60	1.87	1.87	4.53	0.55	1.83	1.83	5.85	1.82	1.83	1.83	3.44	0.48
Γ_1'	3.82	3.82	0.57	0.69	1.73	1.73	0.32	0.82	1.87	1.86	0.32	0.79	1.60	1.59	0.30	0.80
Γ_3'	0.95	0.95	0.13	0.23	1.51	1.52	0.21	0.30	1.90	1.90	0.28	0.44	2.01	2.00	0.34	0.55

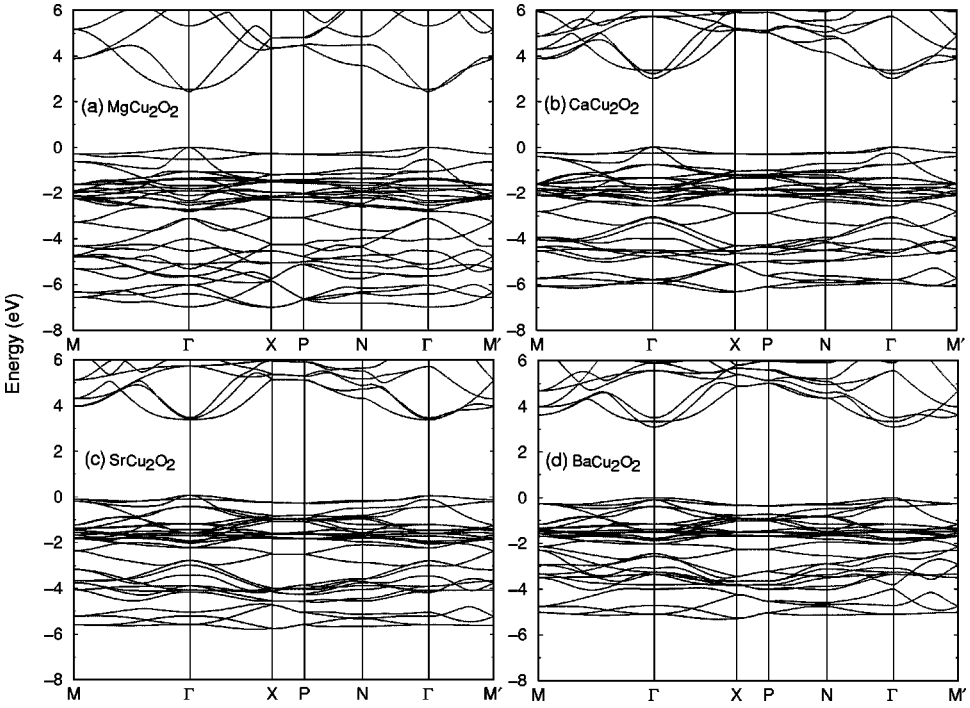

FIG. 5. Calculated semirelativistic electronic band structure for (a) $MgCu_2O_2$, (b) $CaCu_2O_2$, (c) $SrCu_2O_2$, and (d) $BaCu_2O_2$. Energy zero is at VBM. The energy of the conduction bands are shifted upwards by 1.5 eV to correct the LDA band gap error.

of the band gap of $BaCu_2O_2$ relative to $SrCu_2O_2$ is mainly due to the change of the VBM and CBM characters (Fig. 6).

The size effects are studied by changing the lattice parameters of the $A^{II}Cu_2O_2$ compounds from the values for $SrCu_2O_2$ to their respective equilibrium volume. We find that under pressure the Γ_5 state moves up in energy due to increased *d*-*d* and *p*-*d* couplings, that lead to an increase of the crystal field splitting between the Γ_5 and Γ_2 states (see Tables III and IV). Figure 7 shows that variation of the energy levels of the conduction band states with respect to the Γ_5 VBM state. We find that the Γ_1 state with an antibonding *s* character has a large negative deformation potential. Whereas for the Γ_1' and Γ_3' states, which has most of their charge in the interstitial region (similar to the X_1 and X_3 conduction band states in zinc blende semiconductors), the deformation potentials are positive. Thus for $CaCu_2O_2$ the change of volume from that for $SrCu_2O_2$ to its own equilibrium volume pushes the Γ_1 state up and the Γ_1' and Γ_3' states down, so the Γ_1 state is no longer the CBM. Furthermore, we find that dE/du for the Γ_3' and Γ_1 states are positive, while for Γ_1' state it is negative. Therefore, after we relax the *u* parameter to their equilibrium values the Γ_3' states become the CBM for both $MgCu_2O_2$ and $CaCu_2O_2$.

TABLE IV. Calculated angular momentum and site decomposed charge distributions inside the muffin-tin (in percentage) and eigenvalues (in eV) for the VBM and CBM states at Γ. The energy zero is set at the Γ_5 state. All the results are calculated at the experimental lattice constant for $SrCu_2O_2$.

		$MgCu_2O_2$				$CaCu_2O_2$				$SrCu_2O_2$				$BaCu_2O_2$			
		ε	Q_s	Q_p	Q_d	ε	Q_s	Q_p	Q_d	ε	Q_s	Q_p	Q_d	ε	Q_s	Q_p	Q_d
	O	−0.46	0	1	0	−0.19	0	1	0	−0.17	0	2	0	0.13	0	3	0
Γ_2	A^{II}		0	1	0		0	1	0		0	1	0		0	2	0
	Cu		1	0	19		1	0	19		1	0	17		2	0	15
	O	0.00	0	3	0	0.00	0	3	0	0.00	0	4	0	0.00	0	4	0
Γ_5	A^{II}		0	0	0		0	0	0		0	0	0		0	0	0
	Cu		1	0	17		1	0	17		1	0	17		1	0	16
	O	0.35	2	0	0	1.56	2	2	0	1.83	2	2	0	2.30	2	3	0
Γ_1	A^{II}		10	0	0		3	0	0		2	0	0		1	0	0
	Cu		0	0	13		0	0	12		0	0	12		0	0	11
	O	3.96	0	0	0	1.83	0	0	0	1.87	0	0	0	1.49	0	0	0
Γ_1'	A^{II}		0	0	3		0	0	18		0	0	11		0	0	9
	Cu		0	3	0		0	2	0		0	2	0		0	2	0
	O	1.64	0	0	0	1.92	0	2	0	1.90	0	2	0	1.89	0	3	0
Γ_3'	A^{II}		8	0	0		0	0	0		0	0	0		0	0	0
	Cu		0	4	0		0	4	0		0	4	0		0	4	0

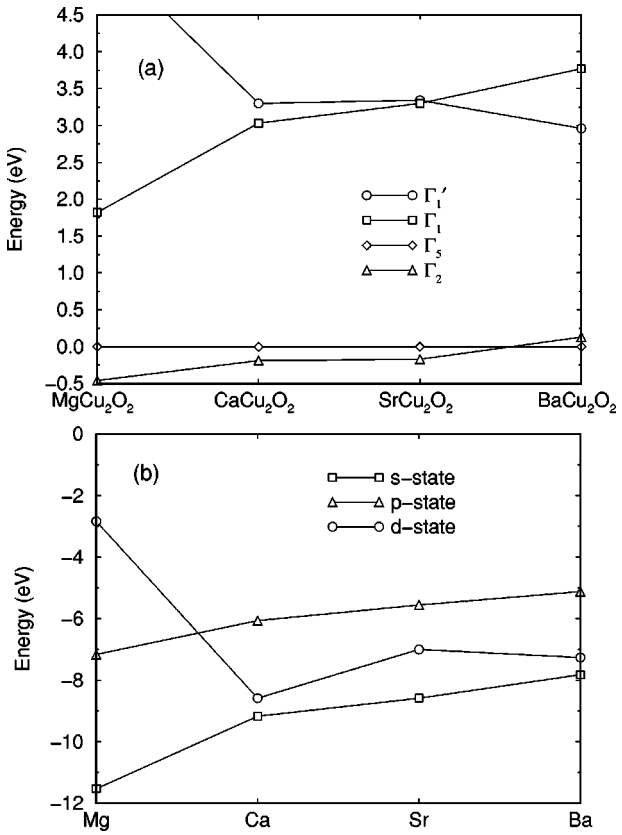

FIG. 6. (a) Variation of the band edge energy levels at Γ as a function of the A^{II} atom for $A^{II}Cu_2O_2$ compounds. The results are calculated at the same experimental lattice constant of $SrCu_2O_2$. (b) Variation of the atomic energy levels of ionized $(A^{II})^+$ atom. Note that the Γ_2 levels trace the A^{II} *p* orbital energies, the Γ_1 levels trace the A^{II} *s* orbital energies, and the Γ_1' level trace the A^{II} *d* orbital energies,

F. Effective mass of the $A^{II}Cu_2O_2$ compounds

We have also calculated the electron and hole effective masses at Γ for states near the band edge of the $A^{II}Cu_2O_2$ compounds. The results shown in Table III are calculated along the Γ-*M* and Γ-*M'* directions. In general, all the $A^{II}Cu_2O_2$ compounds has similar effective masses as for $SrCu_2O_2$. Both the electron and hole effective masses are anisotropic. The hole effective masses perpendicular to c direction at VBM are relatively small for $MgCu_2O_2$, $CaCu_2O_2$, and $SrCu_2O_2$. Due to O mediated coupling between Cu *d* states, the effective masses also decrease when the unit cell volumes decrease from $SrCu_2O_2$ to $CaCu_2O_2$ to $MgCu_2O_2$. This provides another benefit of forming $(Ca_xSr_{1-x})Cu_2O_2$ alloy since the alloy is expected to have smaller hole effective mass, thus, higher electrical conductivity. For $BaCu_2O_2$, however, the VBM hole effective mass along c direction is smaller, and has a different anisotropy from the values for other $A^{II}Cu_2O_2$ compounds. This is because the VBM for $BaCu_2O_2$ is a Γ_2 derived state while for other compounds they are derived from the Γ_5 state.

Our calculated results show that for pure $A^{II}Cu_2O_2$, $SrCu_2O_2$ has the largest band gap, thus is likely to be the most transparent. The band gap could be increased slightly if a small amount of Ca is mixed into $SrCu_2O_2$ to form

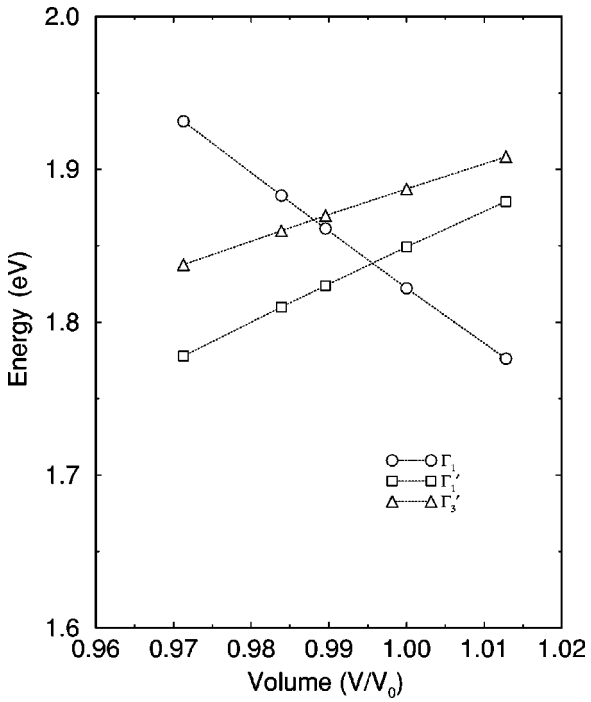

FIG. 7. Calculated conduction energy levels at Γ of $SrCu_2O_2$ as a function of volume (keeping c/a to be constant). The energy zero is set for the Γ_5 state.

$(Ca_xSr_{1-x})Cu_2O_2$ alloys. Using the band gap values in Table III and assume linear interpolation between the corresponding states of $SrCu_2O_2$ and $CaCu_2O_2$, we find the maximum gap is achieved at $x \sim 16\%$. Furthermore, our calculations show that due to larger *p*-*d* and *d*-*d* couplings in $CaCu_2O_2$, its VBM is also slightly higher in energy ($\sim$0.1 eV) than the VBM of $SrCu_2O_2$. Based on the doping limit rule, $CaCu_2O_2$ should be easier to dope *p* type than $SrCu_2O_2$.

V. SUMMARY

In summary, we have systematically studied the electronic and optical properties of *p*-type transparent oxides $A^{II}Cu_2O_2$, where A=Mg, Ca, Sr, and Ba, as well as their host material Cu_2O, using first-principles band structure methods. The trend of band gap variation of $A^{II}Cu_2O_2$ as a function of A^{II} is explained in terms of atomic energy levels and atomic sizes of the A^{II} elements. The calculated dipole matrix elements show that transitions between the VBM and other valence states are negligible within 4 eV below the VBM. This explains the transparencies in these *p*-type TCO's. We predict that adding a small amount of Ca ($\sim$16%) into $SrCu_2O_2$ can increase the band gap and reduce the hole effective mass of $SrCu_2O_2$, therefore, increase the transparency and conductivity.

ACKNOWLEDGMENTS

One of us (X.N.) thanks Dr. G. L. W. Hart and Professor C. Ambrosch-Draxl in using the WIEN97 package. This work was supported by U.S. Department of Energy, Contract No. DE-AC36-99GO10337.

[1] See Review articles in MRS Bull. **25**, No. 8 (2000).
[2] S.B. Zhang, S.-H. Wei, and A. Zunger, J. Appl. Phys. **83**, 3192 (1998).
[3] H. Kawazoe, H. Yanagi, K. Ueda, and H. Hosono, MRS Bull. **25**, No. 8, 28 (2000).
[4] A. Buljan, P. Alemany, and E. Ruiz, J. Phys. Chem. B **103**, 8060 (1999); Chem. Mater. **13**, 338 (2001).
[5] H. Yanagi, S. Inoue, K. Ueda, and H. Kawazoe, J. Appl. Phys. **88**, 4159 (2000).
[6] D. Dubé, B. Champagne, P. Lambert, and Y. Le Page, Mater. Lett. **9**, 353 (1990).
[7] L. Teske and H. Muller-Buschbaum, Z. Anorg. Chem. **379**, 113 (1970).
[8] R. W. G. Wyckoff, *Crystal Structures* (Wiley, New York, 1965).
[9] P. Hohenberg and W. Kohn, Phys. Rev. **136**, B864 (1964); W. Kohn and L.J. Sham, Phys. Rev. **140**, A1133 (1965).
[10] S.-H. Wei and H. Krakauer, Phys. Rev. Lett. **55**, 1200 (1985); D. J. Singh, *Planewaves, Pseudopotentials and the LAPW Method* (Kluwer, Boston, 1994).
[11] A.H. MacDonald, W.E. Pickett, and D.D. Koelling, J. Phys. C **13**, 2675 (1980).
[12] F.D. Murnaghan, Proc. Natl. Acad. Sci. U.S.A. **30**, 244 (1944).
[13] H.J. Monkhorst and J.P. Pack, Phys. Rev. B **13**, 5188 (1976).
[14] D.M. Ceperley and B.J. Alder, Phys. Rev. Lett. **45**, 566 (1980).
[15] J.P. Perdew and A. Zunger, Phys. Rev. B **23**, 5048 (1981).
[16] R. Abt, C. Ambrosch-Draxl, and P. Knoll, Physica B **194-196**, 1451 (1994).
[17] P. Blaha, K. Schwarz, P. Sorantin, and S.B. Trickey, Comput. Phys. Commun. **59**, 399 (1990).
[18] A. Kudo, H. Yanagi, H. Hosono, and H. Kawazoe, Appl. Phys. Lett. **73**, 220 (1998).
[19] R.J. Elliott, Phys. Rev. **108**, 1384 (1957).
[20] W.Y. Ching, Y.-N. Xu, and K.W. Wong, Phys. Rev. B **40**, 7684 (1989).
[21] A. Goltzené, C. Shwab, and H.C. Wolf, Solid State Commun. **18**, 1565 (1976).
[22] A. Goltzené and C. Shwab, Phys. Status Solidi B **92**, 483 (1979).
[23] J.W. Hodby, T.E. Jenkins, C. Shwab, H. Tamura, and D. Trivich, J. Phys. C **9**, 1429 (1976).
[24] E. Ruiz, S. Alvarez, P. Alemany, and R.A. Evarestov, Phys. Rev. B **56**, 7189 (1997).